J Therm Anal Calorim (2017) 129:441–449
DOI 10.1007/s10973-017-6147-1

Effect of salt modification on thermal behavior, immersion heats and methane adsorption properties of chabazite tuff

Meryem Sakizci[1] · Burcu Erdoğan Alver[1]

Received: 28 November 2016 / Accepted: 4 February 2017 / Published online: 15 February 2017

Abstract In this study, the adsorption of methane (CH_4) on chabazite tuff from Bala, Turkey, and that of salt-treated forms (Na^+, K^+, Li^+, Ca^{2+} and Mg^{2+}) was investigated. Structural and thermal characterization of chabazite samples were examined using X-ray diffraction, X-ray fluorescence, thermogravimetry, differential thermal analysis and N_2 adsorption methods. The heats of immersion of the zeolite samples were measured with a Calvet-type C-80 calorimeter. At 30 °C, the Q_{imm} values for heat of immersion decreased in the following order: Mg-CHA (113.62 J g^{-1}) > Li-CHA (112.82 J g^{-1}) > CHA (108.50 J g^{-1}) > Ca -CHA (99.82 J g^{-1}) > Na-CHA (80.00 J g^{-1}) > K-CHA (63.79 J g^{-1}). Adsorption properties of methane for all chabazite samples were obtained at 0 and 25 °C pressures up to 100 kPa. It was found out that CH_4 adsorption capacities of the natural and salt-treated chabazites at 0 °C (0.831–1.315 mmol g^{-1}) were higher than those at 25 °C (0.672–1.163 mmol g^{-1}) as expected.

Keywords Chabazite · Adsorption · Methane · XRD · Thermal analysis · Immersion heat

Introduction

Chabazite (CHA) is naturally occurring zeolite with ideal composition $(Ca_{0.5},Na,K)_4[Al_4Si_8O_{24}]\cdot 12H_2O$ [1]. Aluminosilicate zeolite chabazite with Si/Al ratios of 1–5 has three-dimensional channel system with ellipsoidal-shaped large cavities (6.7 Å × 10 Å) that are accessible via eight-ring windows (3.8 Å × 3.8 Å) [2–4]. The double six-ring unit (D6R) has a free aperture diameter of 0.26 nm [5]. There are five possible cation sites in the dehydrated chabazite. SI is found at the center of the prism (D6R). SII is associated with the double six-ring (D6R) window and is displaced into the ellipsoidal cavity. SIII is close to the corner of the four-ring window of the hexagonal prism [6–10]. SIII′ is located near the center of the ellipsoidal cavity (the eight-ring window) [11]. SIV is near the eight-ring window [12, 13, 18]. Different types of ions have different site preferences and occupancy in these sites. Li^+ resides both SII and SIII. K^+ locates mainly at SIII′ and SIII. Na^+ coordinates the three favorable positions in the order SIII′ > SII > SI [14, 15]. In addition, site SI and site SII are preferentially adopted by Ca^{2+} ions [6, 16].

In many technological processes, the property of zeolites in emitting and absorbing water reversibly is one of the most important and interesting subjects. The intensity of the interaction water molecules with zeolite surfaces can be determined by measurement of heat of immersion. When a solid is immersed into a wetting liquid in which it does not dissolve nor react, it gives some amount of heat [17]. This measured heat is called immersion heat, Q_{imm} (J g^{-1}). Zeolites are minerals that give relatively high immersion heat. Both the surface accessibility of the immersion liquid and the specific interactions between the solid surface and the molecules of liquid are responsible for the total value of the heat of immersion. Many workers have been investigated hydration enthalpy of zeolite from liquid water [18–20]. Because of their high absorption capacities, natural zeolites have been used in various heating and cooling applications. Energy storage is an important part of these applications.

✉ Meryem Sakizci
msakizci@anadolu.edu.tr

[1] Department of Physics, Faculty of Science, Anadolu University, 26470 Eskisehir, Turkey

Methane is a colorless, odorless, flammable and explosive gas that is the simplest alkane and is the principal component of natural gas [21]. It is one of the most damaging greenhouse gases that contributes to potential global warming [22]. CH_4 is emitted from a variety of natural and human-related sources, for example, wetlands, landfills, the oceans and sewers. A large portion of methane emissions are caused by the production, transportation and use of fossil fuels [23]. Therefore, reducing methane emissions will lead to substantial economic and environmental benefits. The chabazite-type zeolites have been applied in industrial adsorption and ion exchange applications. Chabazite zeolite shows a distinct change in its adsorption capacity and surface properties (e.g. surface area, charge) by cation exchanging with different cations [24–26]. The performance of such tailoring, however, rests heavily on the interactions between guest gas molecules and the exchangeable cations. Early investigations exhibited that the effective adsorption pore sizes could be considerably changed by ion exchanging [27–30]. The adsorption of CH_4 on natural and modified zeolites has been reported in various studies [24, 31–49]. However, studies on adsorption of CH_4 based on natural zeolites from Turkey are very limited in the literature. Ackley and Yang [32, 33] determined that uptake of methane on clinoptilolite samples increased in the order $Ca^{2+} < Na^{+} < Mg^{2+} <$ Nat. $< H^{+} < K^{+}$. The adsorption of methane on ion-exchanged clinoptilolite samples at 22 °C was reported by Jayaraman et al. [41]. They determined that CH_4 adsorption capacities of the clinoptilolite samples increased in the following order: $Ca^{2+} < Li^{+} <$ Nat. $< Mg^{2+} < H^{+} = K^{+} < Na^{+}$. Shang et al. [46] investigated the methane adsorption properties of potassium forms of chabazite at 6 °C and found a methane adsorption capacity of 1.97 mmol g^{-1} at 1 MPa.

The novelty of this study is the investigation of the structural, thermal behavior and methane adsorption properties of chabazite zeolites after salt treatment and to evaluate their immersion heats in water using Calvet calorimeter.

Experimental

Materials and methods

The chabazite sample was obtained from the Bala deposit of the Ankara region of Turkey. Chabazite sample was ground and sieved to obtain <45 μm fractions. The chabazite-rich samples were boiled in deionized water (100 mL deionized water for 5 g of chabazite) at 50 °C for 2 h in order to remove the soluble salts. Then, the nitrate solutions were prepared with KNO_3, $LiNO_3$, $NaNO_3$, $Mg(NO_3)_2$ and $Ca(NO_3)_2$ for ion exchange batch experiments. All cationic solutions were intensely shaken using 1 M solutions at 90 °C for 5 h. The treated samples were washed repeatedly with deionized water and dried out in air and then at 110 °C for 16 h before the measurements.

Instrumentation

Prior to the study of methane adsorption, the structural and thermal properties of chabazite-rich mineral and those of salt-treated forms were determined by using XRD, XRF, TG–DTG, DTA and N_2 adsorption techniques. Chemical compositions were obtained on powdered samples fused with lithium tetraborate using X-ray fluorescence analysis (XRF—Rigaku ZSX Primus instrument). Loss on ignition (LOI) was determined from the mass loss after heating the samples to 1000 °C for 2 h. The XRD patterns of all samples were measured on a Bruker AXS powder diffractometer (D8 Advance) using CuK_α radiation ($\lambda = 1.54$ Å) at 40 kV and 20 mA to scan over the 2θ range 3–40°. The samples were scanned at 2θ steps of 0.02°.

Thermal analysis (TG–DTG–DTA) was carried out using a Setsys Evolution Setaram apparatus at a heating rate of 10 °C min^{-1} from 30 to 1000 °C. About 30 mg of the sample was used in each run. The enthalpies of immersion (in water) of the chabazite samples were determined with a Setaram Calvet-type C-80 immersion calorimeter at 30 °C. Prior to the calorimetric experiments, about 400 mg of chabazite sample was heated for 24 h at 150 °C in order to remove the adsorbed water. In these immersion experiments, water was used as immersion liquid for zeolites with hydrophilic surfaces. The whole system is located into the calorimeter, and time is allowed for temperature equilibration between the sample setup and the calorimeter. Once the thermal equilibrium was achieved in calorimeter, the ampoule of sample container was broken and the liquid water allowed to entering into the ampoule and wets sample, the heat flow evolution being monitored as a function of time. Integration of this signal gives the total experimental heat of immersion.

Using a Quantachrome Autosorb 1-C volumetric gas analyzer, the textural properties of the zeolites were measured with N_2 at −196 °C. Previously, the samples were outgassed at 300 °C for 7 h. High-purity nitrogen (99.99%) was used. Surface area of the samples was calculated from the adsorption isotherms according to the Brunauer–Emmett–Teller (BET) method in the range of relative pressure 0.05–0.2 [50]. The micropore surface area and volume were determined using the *t*-plot (de Boer thickness equation) [51]. In addition, total pore volume and average pore diameter values of chabazite samples were obtained using of N_2 adsorption data. CH_4 adsorption isotherms of

the chabazite samples were measured at 0 and 25 °C up to 100 kPa using an Autosorb 1-C gas analyzer. Prior to the adsorption measurements, the samples were degassed by heating at 300 °C under vacuum for 7 h using degassing system Autosorb Turbo. CH_4 with purity of 99.99% was used for adsorption experiments.

Results and discussion

Element composition

The chemical compositions of the natural and that of salt-treated (Na-CHA, K-CHA, Li-CHA, Mg-CHA and Ca-CHA) forms, expressed in terms of oxide species, are given as % mass in Table 1. As Table 1 shows, the major elements of natural chabazite sample were Si, Al, Mg, Ca in addition to small amounts of Na and K.

X-ray analysis

In order to indicate the influence of salt treatment on the structure of chabazite, the X-ray diffraction patterns of all the samples (CHA, Na-CHA, K-CHA, Li-CHA, Mg-CHA, Ca-CHA) are shown in Fig. 1. The XRD pattern of CHA sample indicated that it contained chabazite as the major mineral (characteristic peaks at $2\theta = 9.40°$, 12.76°, 15.90°, 17.78°, 20.48°, 22.98°, 30.50° and 34.39°) with smaller amounts of clinoptilolite (peaks at $2\theta = 9.87°$ and 30.05°) and erionite (peaks at $2\theta = 7.56°$ and 23.56°) [52–54].

There was no appreciable change of the XRD patterns of Mg-CHA and Na-CHA after ion exchange treatment. The powder XRD data and XRF results are consistent in that Mg-CHA has a weaker interaction with the magnesium ions. However, the intensities of reflection observed at 2θ

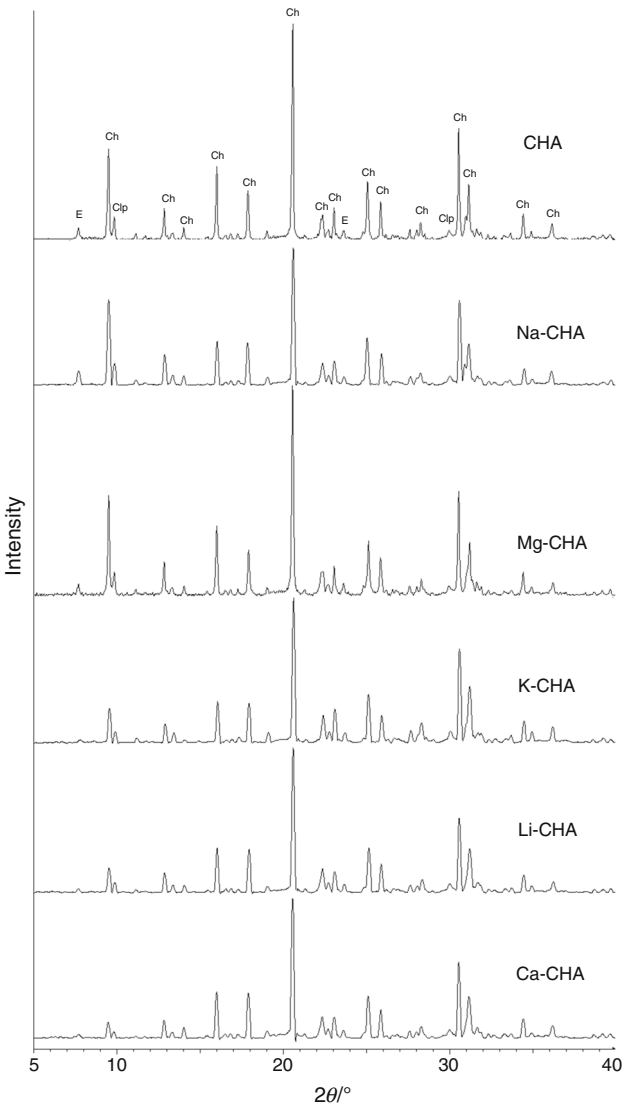

Fig. 1 XRD patterns of the natural and salt-treated chabazites. *Ch* chabazite, *Clp* clinoptilolite, *E* erionite

Table 1 Chemical analyses in oxides (%) for natural and salt-treated chabazite samples

Chemical analysis/%	CHA	Na-CHA	K-CHA	Li-CHA	Ca-CHA	Mg-CHA
SiO_2	57.95	57.87	57.63	59.03	57.74	57.40
Al_2O_3	14.44	14.82	14.64	14.96	14.49	14.44
MgO	3.48	2.47	2.41	2.77	2.38	4.48
CaO	2.37	0.88	0.80	1.86	4.65	1.41
Fe_2O_3	0.92	0.79	0.85	0.80	0.90	0.90
K_2O	1.33	0.92	7.83	1.35	1.23	1.33
Na_2O	1.07	4.45	0.19	0.45	0.30	0.75
TiO_2	0.11	0.07	0.08	0.09	0.10	0.08
P_2O_5	–	0.01	0.01	0.01	0.01	0.01
SrO	0.13	–	–	0.12	0.08	0.12
SO_3	0.01	–	–	0.01	–	–
LOI	18.13	17.67	15.51	18.48	18.04	19.02

values of 9.40°, 15.90°, 20.48° and 30.50° corresponding to the chabazite amount decreased significantly due to the salt treatment with calcium, lithium and potassium solutions. This can be related to cation migration and the elimination of water molecules from the framework channels due to heating.

Specific surface area

The textural properties of all chabazite samples were determined from adsorption isotherms of N_2 at −196 °C and are shown in Fig. 2 and Table 2. The N_2 adsorption isotherms are of the type I [55]. The effect of cation type is clearly seen through the observed adsorption affinities of the salt-treated chabazites.

The BET surface areas decreased in order Li-CHA > Na-CHA > CHA > Ca-CHA > Mg-CHA > K-CHA. It was found that the specific surface areas and micropore volumes of the Li- and Na-exchanged chabazites were high compared to natural chabazite (Table 2). The surface area and micropore volume for Li-CHA were 472 $m^2\ g^{-1}$ and 0.177 $cm^3\ g^{-1}$, respectively, maximum among the studied samples. The high specific surface area of Li-CHA can be ascribed to strong interaction between the nitrogen quadrupole moment and the electrostatic field gradient generated by Li^+ cations [14, 56, 57].

However, the surface areas in the chabazite samples decreased after they were treated with potassium, calcium and magnesium nitrate solutions. It is well known that K^+ ions are weaker adsorption positions as compared to Li^+ and Na^+ ions in the zeolite framework [4, 58, 59]. Previous studies demonstrated that K form of chabazite has a notably reduced effective adsorption pore size because of a massive channel blockage of eight-ring windows [5, 13, 28, 46, 60]. As shown in Table 2, K-CHA gives micropore volume of 0.137 $cm^3\ g^{-1}$ in comparison with 0.174 and 0.177 $cm^3\ g^{-1}$ on Na-CHA and Li-CHA, respectively. The diminished micropore volume corresponds to a low BET surface area of 355 $m^2\ g^{-1}$. The specific surface area of the natural chabazite sample decreased from 446 to 435 $m^2\ g^{-1}$ after treatment with 1 M magnesium nitrate solution. This was likely related to very small ionic radius of Mg^{2+} cations [57, 61].

Thermal properties

Studies on the thermal behavior of chabazite were carried out by several authors [62–74]. The thermal stability of

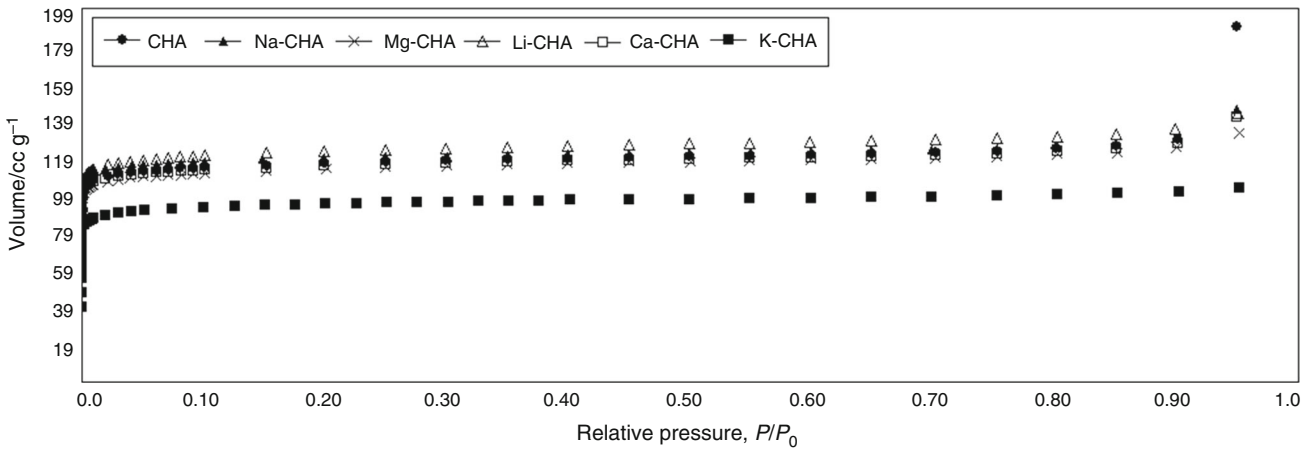

Fig. 2 N_2 adsorption isotherms of natural and salt-treated chabazites

Table 2 Physical properties and CH_4 adsorption capacities of natural and salt-treated chabazite samples

Sample	Amount adsorbed/mmol g^{-1}		BET surface area/$m^2\ g^{-1}$	Micropore volume/$cm^3\ g^{-1}$	Micropore area/$m^2\ g^{-1}$	Total pore volume/$cm^3\ g^{-1}$	Average pore diameter/Å
	0 °C	25 °C					
CHA	0.946	0.761	446	0.167	414	0.295	26.45
Na-CHA	1.315	1.163	458	0.174	430	0.227	19.84
K-CHA	1.162	0.933	355	0.137	330	0.201	22.64
Li-CHA	1.130	0.825	472	0.177	437	0.224	18.94
Ca-CHA	0.831	0.728	441	0.165	407	0.220	19.92
Mg-CHA	0.927	0.672	435	0.161	398	0.207	18.99

chabazite is majorly dependent on the nature of the exchangeable cations [8, 53, 75]. Natural and Li-, Na-, K-, Mg- and Ca-exchanged chabazite samples were characterized by a single endothermic peak with a minimum at about 200 °C, which was ascribed to the loss of hydroscopic and zeolitic water (Fig. 3). Endotherm minima temperatures increase in the sequence: K-CHA (190 °C) → Ca-CHA (192 °C) → Na-CHA (197 °C) → CHA (202 °C) → Li-CHA (203 °C) → Mg-CHA (213 °C). These results are similar to those reported by Barrer and Langley [65]. They showed that chabazite samples are characterized by a large endothermic peak extending from room temperature to about 400 °C. In addition, these samples was characterized by a very sharp exothermic peak at about 880–930 °C. This exothermic peak shows an irreversible structural change in the zeolite samples.

The TG curves for the natural and salt-treated chabazite samples exhibited a rather smooth and similar curve (Fig. 3). Breck demonstrated that intracrystalline zeolitic water in chabazite is removed continuously and reversibly [5]. In this study, the thermogravimetric curves show that water losses of chabazite samples are nearly complete at temperatures approaching 400 °C, but continue very slowly up to 1000 °C. The mass loss of this temperature reaches 11.04–14.42% (Table 3). The destruction of the

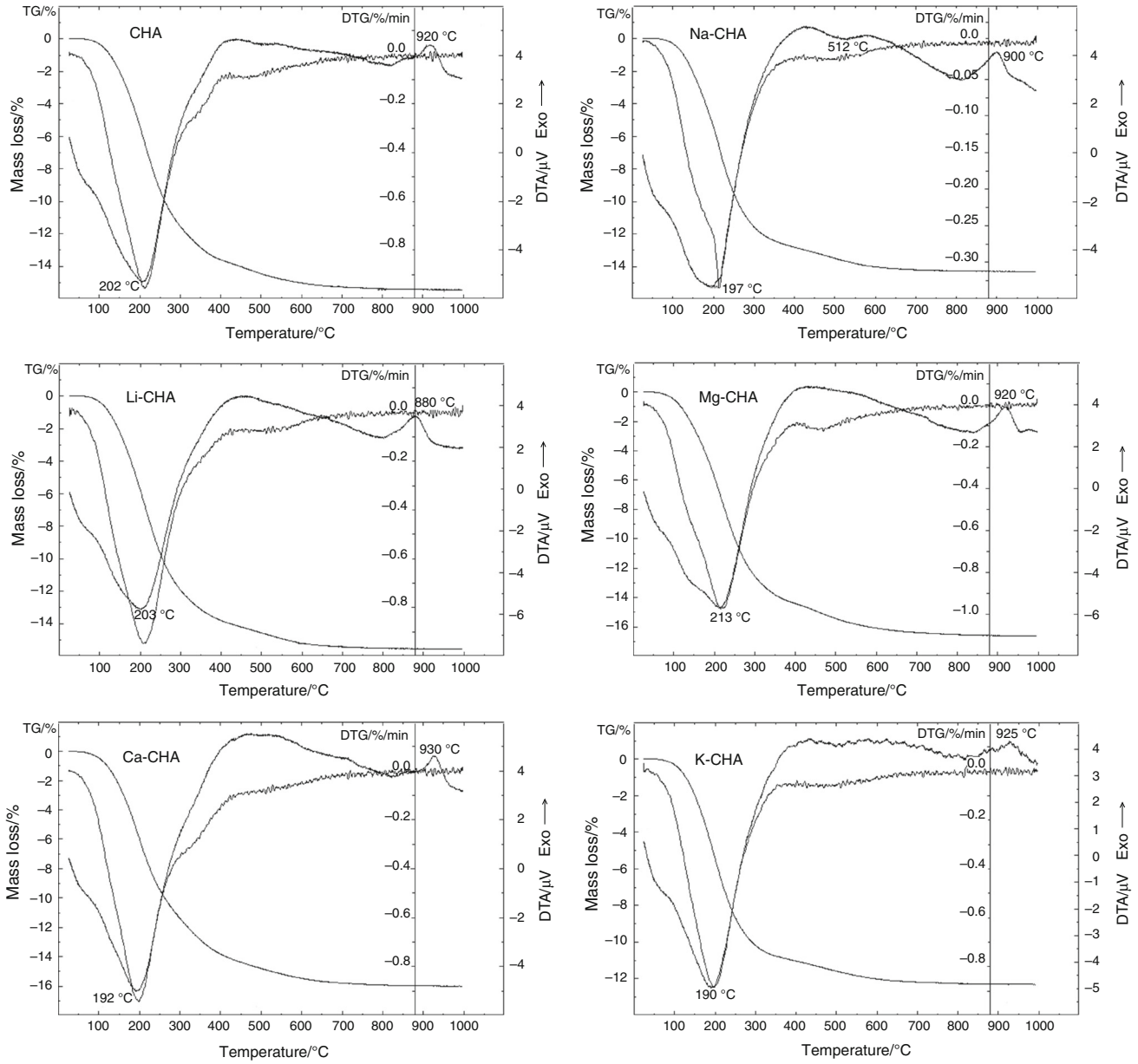

Fig. 3 TG–DTG and DTA curves for the natural and salt-treated chabazites

Table 3 Mass loss (%) of the natural and salt-treated chabazites used at different temperature ranges

Sample	30–100 °C	100–200 °C	200–300 °C	300–400 °C	400–500 °C	500–600 °C	600–700 °C	700–1000 °C	Total mass loss/%
CHA	0.33	5.10	6.15	2.03	0.84	0.57	0.25	0.16	15.43
Na-CHA	0.31	5.15	6.11	1.26	0.67	0.52	0.17	0.10	14.29
K-CHA	0.32	5.17	4.70	0.85	0.55	0.42	0.16	0.12	12.29
Li-CHA	0.37	5.45	6.14	1.86	0.75	0.63	0.23	0.11	15.54
Ca-CHA	0.47	5.58	4.92	2.42	0.96	0.67	0.32	0.20	15.99
Mg-CHA	0.51	5.31	6.76	1.84	1.03	0.65	0.29	0.23	16.62

structure begins only after 700 °C and quickly completed within a short temperature range. The total mass loss while heating zeolite up to 700 °C is 12.17–16.39%. The Mg-exchanged chabazite gave the highest rate of mass loss (Table 3).

Heats of immersion

The heats of immersion of Na-, K-, Li-, Ca- and Mg-exchanged chabazite samples have been determined by Calvet calorimeter. The calorimetric results for these samples are expressed in terms of the heat evolved (Q_{imm}) (Table 4). The results obtained for the immersion heats showed values between 63.79 and 113.62 J g^{-1} for water. At 30 °C, the Q_{imm} values for heat of immersion decreased in the following order: Mg-CHA > Li-CHA > CHA > Ca-CHA > Na-CHA > K-CHA.

The results showed that the heats of immersion in water (in J g^{-1}) for modified chabazite with magnesium and lithium increased compared to natural chabazite. For Ca-CHA, Na-CHA and K-CHA samples, the heats of immersion in water decreased. In general, the value of the heat of immersion is proportional to the surface area. Modifications of chabazites affected the specific surface area and as a consequence the heat of immersion in water. K-CHA is characterized by significantly decreased value of surface area because of larger size of cation than the other cations. This caused a decrease in the heat of immersion in water. In addition, the heat of immersion in water on ion-exchanged forms decreased with increasing cation radius. The presented values are generally the average values of three experiments.

Table 4 Immersion heats of the natural and salt-treated chabazites

Sample	Q_{imm}/J g^{-1}
CHA	108.50
Na-CHA	80.00
K-CHA	63.79
Li-CHA	112.82
Ca-CHA	99.82
Mg-CHA	113.62

Adsorption of CH_4

The CH_4 adsorption isotherms of CHA and salt-treated chabazite samples (Na-CHA, K-CHA, Li-CHA, Mg-CHA and Ca-CHA) were measured at 0 and 25 °C and pressures up to 100 kPa using a static volumetric system. These two temperatures employed are above the critical temperature for CH_4 ($T_c = -82.6$ °C). CH_4 adsorption isotherms of all samples are shown in Figs. 4 and 5. The absolute amounts adsorbed per gram of natural and salt-treated chabazites are given in Table 2. The maximum CH_4 adsorption capacity of all forms of chabazite samples ranged from 0.672 to 1.315 mmol g^{-1}. Methane (3.8 Å) [76] can enter into the pore openings of chabazite (about 4.9 Å) [28].

At 25 °C, the adsorption capacity of CH_4 at 100 kPa is in the sequence Na-CHA > K-CHA > Li-CHA > CHA > Ca-CHA > Mg-CHA, and at 0 °C, this becomes sequence Na-CHA > K-CHA > Li-CHA > CHA > Mg-CHA > Ca-CHA. At 0 °C, the amount of CH_4 retained by the natural chabazite (CHA) was 0.946 mmol g^{-1}, whereas the corresponding value was 0.761 mmol g^{-1} at 25 °C. Na-, K- and Li-exchanged chabazite showed increase in methane adsorption capacity. Of all salt-treated chabazites, Na form exhibited the best properties in terms of adsorption capacity at both temperatures studied. The significant increase in adsorption capacity of CH_4 on Na-CHA was

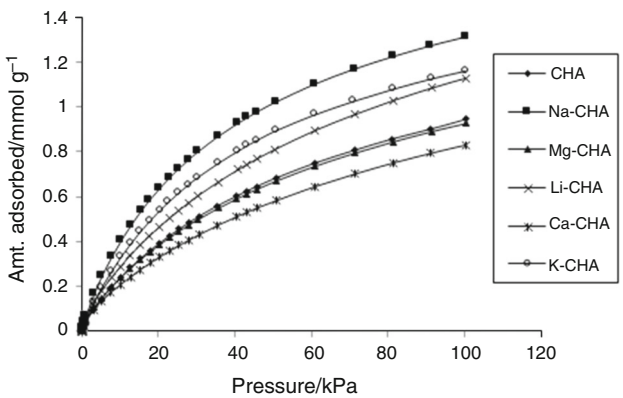

Fig. 4 CH_4 adsorption isotherms of natural and salt-treated chabazites at 0 °C

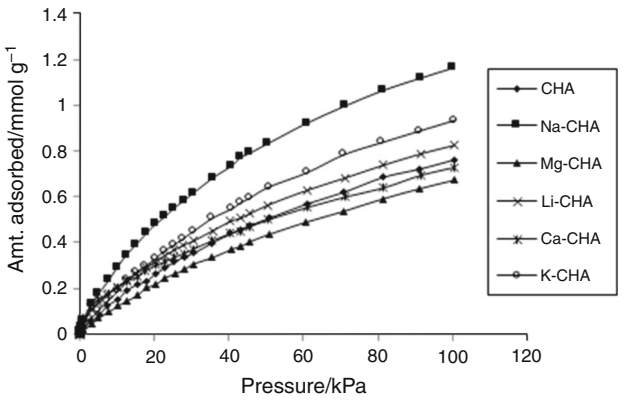

Fig. 5 CH_4 adsorption isotherms of natural and salt-treated chabazites at 25 °C

mainly due to effective dispersion interactions between methane and chabazite structure. Thus, as shown in Table 2, the adsorption capacity of CH_4 on Na-CHA increased from 1.163 to 1.315 mmol g^{-1} as the temperature decreased from 25 to 0 °C. For sample Li-CHA, the amount of CH_4 adsorbed increased from 0.825 to 1.130 mmol g^{-1} on decreasing the temperature from 25 to 0 °C. K-CHA sample demonstrated higher adsorption capacity of CH_4 relative to the natural chabazite sample (Table 4). This is likely related to the large K^+ atomic diameter. K^+ has the biggest atomic diameter compared to the other cations. The low shielding of big cations by CH_4 molecules increases their electrostatic interactions, and so they can strongly interact with CH_4 molecules. From 25 to 0 °C at 100 kPa, CH_4 adsorption amount is increased from 0.933 to 1.162 mmol g^{-1} for K-CHA. The total pore volume of Na-CHA (0.227 cm^3 g^{-1}) is larger than that of K-CHA (0.201 cm^3 g^{-1}). This accounts for the larger adsorption capacity in Na-CHA at higher pressure.

The chabazite samples treated with calcium and magnesium nitrate solutions had the lowest methane adsorption capacities at both temperatures. The shielding of cations by CH_4 molecules increases with decrease in cation size. Therefore, the decrease in methane adsorption capacity on Mg-CHA was because of the decrease in interaction between Mg^{2+} cations and CH_4 molecules [61]. At 0 °C, Mg-CHA has higher charge density than Ca-CHA which explains the greater Ca-CHA capacity. Ca-exchanged chabazite showed methane adsorption capacity of 0.831 mmol g^{-1} at 0 °C and 100 kPa pressure, minimum among the studied samples.

Conclusions

- Based on X-ray patterns, the characteristic peaks of Mg-CHA and Na-CHA remained essentially unchanged with only small reduction in peak intensity compared to natural chabazite sample. However, the most characteristic peaks of chabazite decreased considerably with salt treatment with calcium, lithium and potassium solutions.
- The natural and salt-treated chabazite samples showed similar thermal behavior. The DTA curves of all forms of chabazite samples exhibited a single endothermic peak at 190–213 °C between 30 and 400 °C due to the loss of hydroscopic and zeolitic water. In addition, these samples displayed a rather sharp exothermic peak at 880–930 °C corresponding to the irreversible structural changes in the zeolite samples.
- The heat of immersion (in water) was determined with a Calvet calorimeter for chabazite samples. Mg-CHA sample exhibited the highest Q_{imm} value (113.62 J g^{-1}) among the modified zeolites.
- Among ion-exchanged chabazite samples, it was found that the Na-CHA had the highest methane adsorption capacity at both temperatures. However, the samples with alkaline earth cations (Mg^{2+} and Ca^{2+}) showed a lower methane adsorption capacity than the natural and alkali-exchanged chabazite samples (Na^+, K^+ and Li^+) due to decrease in the electrostatic and polarization interactions. Sodium ion-exchanged chabazite tuff appeared to be a particularly suitable adsorbent for the removal of CH_4.

Acknowledgements This work was supported by Anadolu University Commission of Scientific Research Project under Grant No. 1002F87. Special thanks to Dr. Matthias Thommes for his helpful suggestions.

References

1. Bish DL, Ming DW. Natural zeolites: occurrence, properties, applications. In: Bish DL, Ming DW, editors. Reviews in mineralogy and geochemistry. Washington: Mineralogical Society of America; 2001. p. 1–57.
2. Kington GL, Laing W. The crystal structure of chabazite and its sorptive properties. Trans Faraday Soc. 1955;51:287–98.
3. Meier WM, Olson DH. Atlas of zeolite structure types. Zeolites. 1992;12:449–656.
4. Keffer D, Davis HT, McCormick AV. The effect of nanopore shape on the structure and isotherms of adsorbed fluids. Adsorption. 1996;2:9–21.
5. Breck DW. Zeolite molecular sieves: structure, chemistry and use. New York: Wiley; 1974.
6. Mortier MJ, Pluth JJ, Smith JV. Positions of cations and molecules in zeolites with the chabazite framework. I. Dehydrated Ca-exchanged chabazite. Mater Res Bull. 1977;12:97–102.
7. Mortier MJ, Pluth JJ, Smith JV. Positions of cations and molecules in zeolites with the chabazite-type framework. III. Dehydrated Na-exchanged chabazite. Mater Res Bull. 1977;12:241–50.
8. Alberti A, Galli E, Vezzaleni G, Passaglia E, Zanazzi PF. Position of cations and water molecules in hydrated chabazite. Natural and Na-, Ca-, Sr- and K-exchanged chabazites. Zeolites. 1982;2:303–9.

9. Calligaris M, Mezetti A, Nardin G, Randaccio L. Cation sites and framework deformations in dehydrated chabazites. Crystal structure of a fully silver-exchanged chabazite. Zeolites. 1984;4:323–8.
10. Calligaris M, Mezetti A, Nardin G, Randaccio L. Crystal structures of the hydrated and dehydrated forms of a partially cesium-exchanged chabazite. Zeolites. 1986;6:137–41.
11. Nakatsuka A, Okada H, Fujiwara K, Nakayama N, Mizota T. Crystallographic configurations of water molecules and exchangeable cations in a hydrated natural CHA-zeolite (chabazite). Microporous Mesoporous Mater. 2007;102:188–95.
12. Smudde GH, Slager TL, Coe CG, MacDougall JE, Weigel SJ. DRIFTS and raman investigation of N_2 and O_2 adsorption on zeolites at ambient temperature. Appl Spectrosc. 1995;49:1747–55.
13. Ridha FN, Yang Y, Webley PA. Adsorption characteristics of a fully exchanged potassium chabazite zeolite prepared from decomposition of zeolite Y. Microporous Mesoporous Mater. 2009;117(1–2):497–507.
14. Smith LJ, Eckert H, Cheetham AK. Site preferences in the mixed cation zeolite, Li, Na-Chabazite: a combined solid-state NMR and neutron diffraction study. J Am Chem Soc. 2000;122:1700–8.
15. Smith LJ, Eckert H, Cheetham AK. Potassium cation effects on site preferences in the mixed cation zeolite: Li, Na-chabazite. Chem Mater. 2001;13:385–91.
16. Grey T, Gale J, Nicholson D, Peterson B. A computational study of calcium cation locations and diffusion in chabazite. Microporous Mesoporous Mater. 1999;31:45–59.
17. Everett DH. Definitions, terminology and symbols in colloid and surface chemistry. Pure Appl Chem. 1972;31(4):579–638.
18. Petrova N, Kirov D. Heats of immersion of clinoptilolite and its ion-exchanged forms: a calorimetric study. J Therm Anal Calorim. 1995;43:323–7.
19. Petrova N, Mizota T, Fujiwara K. Hydration heats of zeolites for evaluation of heat exchangers. J Therm Anal Calorim. 2001;64(1):157–66.
20. Carey JW, Bish DL. Equilibrium in the clinoptilolite-H_2O system. Am Mineral. 1996;81:952–62.
21. Cardarelli F. Materials handbook: a concise desktop reference. 2nd ed. London: Springer; 2008.
22. Shindell DT, Faluvegi G, Koch DM, Schmidt GA, Unger N, Bauer SE. Improved attribution of climate forcing to emissions. Science. 2009;326:716–8.
23. Inventory of U.S. Greenhouse gas EPA. Emissions and sinks: 1990–2012. 15, 2014.
24. Huesca RH, Diaz L, Armenta GA. Adsorption equilibria and kinetics of CO_2, CH_4 and N_2 in natural zeolites. Sep Purif Technol. 1999;15:163–73.
25. Roque-Malherbe RMA. Adsorption and diffusion in nanoporous materials. Boca Raton: CRC Press; Taylor & Francis; 2007.
26. Karger J. Single-File Diffusion in Zeolites. In: Karge HG, Weitkamp J, editors. Molecular Sieves: Adsorption and Diffusion. Berlin: Springer; 2008. p. 329–366.
27. Barrer RM. Specificity in physical sorption. J Colloid Interface Sci. 1966;21:415–34.
28. Barrer RM. Zeolites and clay minerals as sorbents and molecular sieves. New York: Academic Press; 1978.
29. Ackley MW, Yang RT. Adsorption characteristics of high-exchange clinoptilolites. Ind Eng Chem Res. 1991;30:2523–30.
30. Yang RT. Adsorbents: fundamentals and applications. Hoboken: Wiley; 2003.
31. Munson RA, Clifton RA Jr. Natural gas storage with zeolites, USA: Bureau of Mines Nonmetallic Minerals Program. Washington: U.S. Department of the Interior; 1971.
32. Ackley MW, Yang RT. Diffusion in Ion-exchanged Clinoptilolites. AIChE J. 1991;37(11):1645–56.
33. Ackley MW, Yang RT. Adsorption characteristics of high-exchange clinoptilolites. Ind Eng Chem Res. 1991;30(12):2523–30.
34. Ackley MW, Giese RF, Yang RT. Clinoptilolite: an untapped potential for kinetic gas separations. Zeolites. 1992;12:780–7.
35. Predescu L, Tezel FH, Stelmack P. Adsorption of nitrogen and methane on natural clinoptilolite. In: Bonneviot L, Kaliaguin S, editors. Zeolites: a refined tool for designing catalytic sites. Amsterdam: Elsevier; 1995. p. 507–12.
36. Menon VC, Komarneni S. Porous adsorbents for vehicular natural gas storage: a review. J Porous Mater. 1998;5:43–58.
37. Nagano J, Eguchi T, Asanuma T, Masui H, Nakayama H, Nakamura N, Derouane EG. ^{1}H and ^{129}Xe NMR investigation of the microporous structure of dealuminated H-mordenite probed by methane and xenon. Microporous Mesoporous Mater. 1999;33:249–56.
38. Macedonia MD, Moore DD, Maginn EJ, Olken MM. Adsorption studies of methane, ethane, and argon in the zeolite mordenite: molecular simulations and experiments. Langmuir. 2000;16:3823–34.
39. Aguilar-Armenta G, Hernandez-Ramirez G, Flores-Loyola E, Ugarte-Castaneda A, Silva-Gonzalez R, Tabares-Munoz C, Jimenez-Lopez A, Rodriguez-Castellon E. Adsorption kinetics of CO_2, O_2, N_2, and CH_4 in cation-exchanged clinoptilolite. J Phys Chem B. 2001;105:1313–9.
40. Aguilar-Armenta G, Patiño-Iglesias ME, Leyva-Ramos R. Adsorption kinetic behavior of pure CO_2, N_2 and CH_4 in natural clinoptilolite at different temperatures. Sci Technol. 2003;21:81–91.
41. Jayaraman A, Hernandez-Maldonado AJ, Yang RT, Chinn D, Munson CL, Mohr DH. Clinoptilolites for nitrogen/methane separation. Chem Eng Sci. 2004;59:2407–17.
42. Delgado JA, Uguina MA, Gómez JM, Ortega L. Adsorption equilibrium of carbon dioxide, methane and nitrogen onto Na and H-mordenite at high pressures. Sep Purif Technol. 2006;48:223–8.
43. Kouvelos E, Kesore K, Steriotis T, Grigoropoulou H, Bouloubasi D, Theophilou N, Tzintzos S, Kanelopoulos N. High pressure N_2/CH_4 adsorption measurements in clinoptilolites. Microporous Mesoporous Mater. 2007;99:106–11.
44. Faghihian H, Talebi M, Pirouzi M. Adsorption of nitrogen from natural gas by clinoptilolite. J Iran Chem Soc. 2008;5:394–9.
45. Sun Y, Liu C, Su W, Zhou Y, Zhou L. Principles of methane adsorption and natural gas storage. Adsorption. 2009;15:133–7.
46. Shang J, Li G, Singh R, Xiao P, Liu JZ, Webley PA. Potassium chabazite: a potential nanocontainer for gas encapsulation. J Phys Chem C. 2010;114:22025–31.
47. Erdoğan-Alver B, Sakızcı M. Influence of acid treatment on structure of clinoptilolite tuff and its adsorption of methane. Adsorption. 2015;21:391–9.
48. Sakızcı M. Study of thermal and CH_4 adsorption properties. J Therm Anal Calorim. 2015;22:611–20.
49. Sakızcı M, Özgül-Tanrıverdi L. Influence of acid and heavy metal cation exchange treatments on methane adsorption properties of mordenite. Turk J Chem. 2015;39:970–83.
50. Brunauer S, Emmett PH, Teller E. Adsorption of gases in multi molecular layers. J Am Chem Soc. 1938;60:309–19.
51. Lippens BC, de Boer JH. Studies on pore systems in catalysts–V. The t method. J Catal. 1965;4:319–23.
52. Passaglia E. The crystal chemistry of chabazites. Am Mineral. 1970;55:1278–301.
53. Calligaris M, Nardin G, Randaccio L. Cation site location in hydrated chabazites. Crystal structure of potassium- and silver-exchanged chabazites. Zeolites. 1983;3:205–8.
54. Gottardi G, Galli E. Minerals and rocks: natural zeolites. Berlin: Springer; 1985.

55. Gregg SJ, Sing KSW. Adsorption, surface area and porosity. 2nd ed. London: Academic Press; 1982.
56. Papai I, Goursot A, Fajula F, Plee D, Weber J. Modeling of N_2 and O_2 adsorption in zeolites. J Phys Chem. 1995;99:12925–32.
57. Gaffney TR. Porous solids for air separation. Curr Opin Solid State Mater Sci. 1996;1:69–75.
58. James SD. Electrochemistry of the interface between some aluminosilicate crystals and salt solutions. I. Surface conductivity. J Phys Chem. 1966;70(11):3447–54.
59. Pluth JJ, Smith JV, Mortier WJ. Positions of cations and molecules in zeolites with the chabazite framework. IV. Hydrated and dehydrated Cu^{2+} exchanged chabazite. Mater Res Bull. 1977;12:1001–7.
60. Cartlidge S, Keller EB, Meier WM. Role of potassium in the thermal stability of CHA- and EAB-type zeolites. Zeolites. 1984;4:226–30.
61. Sethia V, Somani RS, Bajaj HC. Adsorption of carbon monoxide, methane and nitrogen on alkaline earth metal ion exchanged zeolite-X: structure, cation position and adsorption relationship. RSC Adv. 2015;5:12773–81.
62. Koizumi M. The differential thermal analysis curves and the dehydration curves of zeolites. Mineral J. 1953;1:36–47.
63. Mason B, Greenberg SS. Zeolites and associated minerals from Southern Brazil. Ark Mineral Geol. 1954;1:519–26.
64. Barrer RM, Baynham JW. Synthetic chabazites: correlation between isomorphous replacements, stability, and sorption capacity. J Chem Soc. 1956:2892–2903.
65. Barrer RM, Langley DA. Reactions and stability of chabazite-like phases. Part I. Ion-exchanged forms of natural chabazite. J Chem Soc. 1958:3804–3811.
66. Barrer RM, Langley DA. Reactions and stability of chabazite-like phases Part II. Ion-exchanged forms of some synthetic species. J Chem Soc. 1958:3811–3816.
67. Barrer RM, Langley DA. Reactions and stability of chabazite-type phases. Part III. Intracrystalline water. J Chem Soc. 1958:3817–3824.
68. Pecsi-Donath E. On the individual properties of some Hungarian zeolites. Acta Geol Hung. 1965;9:235–57.
69. Barrer RM, Cram PJ. Heats of immersion of outgassed and ion-exchanged zeolites. In: Flanigen EM, Sand LB, editors. Molecular sieve zeolites, vol. II. Washington: American Chemical Society; 1971. p. 105–31.
70. Valueva GP, Goryainov SV. Chabazite during dehydration: thermochemical and Raman spectroscopy study. Russian Geol Geophys. 1992;33(12):68–75.
71. Drebushchak VA. Measurements of heat of zeolite dehydration by scanning heating. J Therm Anal Calorim. 1999;58:653–62.
72. Shim SH, Navrotsky A, Gaffney TR, MacDougall JE. Chabazite: energetics of hydration, enthalpy of formation, and effect of cations on stability. Am Mineral. 1999;84:1870–82.
73. Bish DL, Carey JW. Thermal behavior of natural zeolites. In: Bish DL, Ming DW, editors. Natural zeolites: occurrence, properties, applications. Rev Mineral Geochem: Washington; 2001. p. 403–52.
74. Ogorodova LP, Kiseleva IA, Mel'chakova LV, Belitskii IA. Thermodynamic properties of calcium and potassium chabazites. Geochem Int. 2002;40:466–71.
75. Calligaris M, Nardin G, Randaccio L. Cation site location in a natural chabazite. Acta Cryst B. 1982;38:602–5.
76. Lide DR. CRC handbook of chemistry and physics. Boca Raton: CRC Press; 2003.